The effects of quench rate and pre-deformation on precipitation hardening in Al-Mg-Si alloys with different Cu amounts

Takeshi Saito[1,*], Calin D. Marioara[2], Jostein Røyset[3], Knut Marthinsen[4] and Randi Holmestad[1]

[1]Department of Physics, Norwegian University of Science and Technology, N-7491 Trondheim, Norway
[2]SINTEF Materials and Chemistry, N-7465 Trondheim, Norway
[3]Hydro Aluminum Research and Technology Development, N-6601 Sunndalsøra, Norway
[4]Department of Materials Science and Engineering, Norwegian University of Science and Technology, N-7491 Trondheim, Norway

*corresponding author
Email: takeshi.saito@ntnu.no
Phone number: +47 73 59 07 30
Postal address: Høgskoleringen 5, Realfagbygget, 7491 Trondheim, Norway

Abstract

The effects of quench rate after solution heat treatment in combination with 1% pre-deformation on precipitation hardening in three Al-Mg-Si alloys have been investigated by transmission electron microscopy and hardness measurements during an isothermal heat treatment. The alloys contain different Cu amounts (up to 0.1 wt%) and the same amounts of other solute elements. While a Cu amount below 0.01wt% does not affect precipitation hardening, an addition of 0.1wt% Cu increases hardness due to formation of a fine microstructure having a high number density of short precipitates. A double peak hardness evolution was observed during isothermal heat treatment. This effect was most pronounced for alloys with low quench rate, and less pronounced for alloys with 1% pre-deformation and 0.1wt% Cu addition. The low quench rate also led to wider precipitation free zones. This effect was also less pronounced by 1% pre-deformation and addition of 0.1wt% Cu.

Keywords
aluminum alloys; hardness measurement; electron microscopy; thermomechanical processing; age hardening; phase transformation

1. Introduction

The 6xxx series of Al alloys (i.e. Al-Mg-Si alloys) are predominant heat-treatable materials used in a wide range of industrial applications. A commercial interest in the 6xxx series has strongly been attracted on the basis of their characteristic properties: high strength-to-weight ratio, good formability and high corrosion resistance. Their main specific feature is a significant increase in hardness due to formation of a large number of nano-sized, (semi-)coherent, metastable precipitates during isothermal heat treatment, which yield interfacial strain into the Al matrix. The interfacial strain eventually makes dislocations shearing and/or looping on precipitates to prevent their movements (the latter is known as the Orowan mechanism [1]), depending on size and distribution of precipitates. Hence, mechanical properties of the alloys depend highly on the microstructure. The precipitates form in alloys with relatively low amounts of solute elements (typically up to a total of 2 wt% of Mg and Si) which become supersaturated in the Al lattice after solution heat treatment. Quenching (rapid cooling) from the solution heat treatment creates quenched-in vacancies which promote diffusion of solute elements into clusters and their growth into metastable precipitates during the following isothermal heat treatment.

The precipitation sequence in the Al-Mg-Si alloys is as follows [2-10]:

SSSS → atomic clusters → GP zones (pre-β") → β"→ β', U1 (Type-A), U2 (Type-B), B' (Type-C) → β, Si

where SSSS stands for super saturated solid solution. The main hardening precipitates are the highly-coherent, needle-shaped GP zones and β" which form the finest microstructure at peak hardness. The post-β" phases are semi-coherent rods/laths and produce coarser precipitate microstructures with a lower strength contribution. All needles/rods/laths have their main growth direction along <001>Al. The precipitate microstructure and types are determined by alloy composition and thermo-mechanical treatment.

It was previously demonstrated [11] that a low Cu addition (~0.1 wt%) does not alter the precipitation sequence in the Al-Mg-Si alloy system, although this level of Cu leads to higher strength by means of forming a higher number density of shorter precipitates having a partially disordered structure [11, 12]. Aluminum recycling is increasing. Since Cu is one of the trace elements that can be accumulated in the scrap base during recycling, it is relevant to investigate the effects of low Cu additions.

The SSSS is reached when the alloy is solution heat treated and subsequently cooled or quenched to room temperature at a rate fast enough to avoid significant precipitation. It has previously been reported that slow quench rates influence the formation of grain boundary precipitates [13] and cause an increase in the width of precipitate free zone (PFZ), leading to intergranular fracture [14] in some Al-Mg-Si alloys. Slower quench rates also lead to lower strength [15] because of loss of quenched-in vacancies [16] which are essential for the atomic diffusion during precipitation and their concentration decides the precipitation hardening behavior [17-20]. It was recently demonstrated [21] that quenching into temperatures ~160°C (interrupted quenching) enhances precipitation kinetics and increases overall hardness due to an increase in mobile vacancies which promotes clusters transforming to β". Another report [22]

showed that slow cooling leads to less precipitate number densities because of loss of quenched-in vacancies. Although natural aging (room temperature storage before the isothermal heat treatment) time generally influences the type of atomic clusters and consequently mechanical properties after precipitation [23, 24], the slow cooling leads to lower influences on the effects of natural aging [22]. Investigations of effects of quench rates are important since a fast quenching is not always possible in industrial processes because of e.g. limitations of the production equipment, or restrictions on shape changes that may be introduced by residual stress if the materials are quenched.

It is known that deformation between solution heat treatment and artificial aging affects precipitation. Since the deformation is conducted before further isothermal heat treatment, it is called "pre-deformation". Nucleation rates and precipitation kinetics are enhanced since the pre-deformation decreases activation energy of the growth of precipitates [25, 26]. It has been reported [27-31] that 10%-15% pre-deformation leads to formation of heterogeneous nucleation along dislocation lines. After artificial aging, different types of precipitates (except for β") form: a continuous decoration of the dislocation lines ("string-like" precipitates) together with discrete precipitation consisting mainly of B' [27-30], and together with (often disordered) Q' [11, 12, 31, 32] if Cu is present in the Al-Mg-Si alloys. In the case of 0.5%-5% pre-deformation, β" is dominant at peak hardness condition, and this level of pre-deformation accelerates formation of β" due to decreased activation energy [33-36]. This can be attributed to the fact that formation of atomic clusters transforming to β" is enhanced during natural aging due to the pre-deformation [37]. Investigation of ~1% pre-deformation is relevant in industrial practice where the pre-deformation is applied to straighten the workpiece, e.g. after extrusion.

The effects of low Cu additions, quench rates and pre-deformation on precipitation hardening in Al-Mg-Si alloys must be due to modified atomic diffusion rates and quenched-in vacancy concentrations during thermo-mechanical treatment. The objective of the present work is hence how these factors influence the precipitation hardening. In this study, the effects of low Cu additions (up to 0.1 wt%), quench rates and 1% pre-deformation on precipitation hardening in Al-Mg-Si alloys have been systematically investigated by hardness measurements and transmission electron microscopy (TEM).

2. Experimental procedure

Three alloys with different amounts of Cu (0.001, 0.01 and 0.1 wt%), but with fixed levels of Mg and Si, were used. The alloy compositions were measured by inductively coupled plasma optical emission spectroscopy and are shown in Table 1. Hereafter the alloys with different increasing amounts of Cu will be referred to as LC1, LC2 and LC3, respectively, as shown in Table 1. Although the three alloys contain Fe, the level (~0.07 wt%) was considered to be representative for the lowest practical Fe-level to be expected in industrial alloys. The alloys were cast as Ø95mm cylindrical ingots, from which extrusion billets were cut. The billets were homogenized at 575°C for 2.5 hours and cooled. The billets were subsequently extruded to Ø20mm round profiles. The extrusion was conducted using a direct press and a single hole die. The billet preheating temperature was 500~510°C which was well above the solvus temperature for the alloys, and the extruded profiles were water-quenched approximately 5 seconds after the die exit. The extruded profiles were cut into lengths of 50 cm. Hence, all the samples were round

bars with Ø20mm in length of 50 cm. The samples were solution heat treated at 540°C for 1 hour in an air circulation oven. There were four different thermo-mechanical treatments conducted after the solution heat treatment: (a) water quenching (b) slow cooling (the cooling rate was 85°C/min until 200°C was reached, and then the sample was quenched), (c) water quenching and then 1% pre-deformation after 30 minutes and (d) slow cooling and 1% pre-deformation after 30 minutes. Hereafter these conditions will be referred to as conditions (a), (b), (c) and (d), respectively, as shown in Figure 1. The cooling rate in conditions (b) and (d) were measured by a K-type thermo couple in the middle of the samples. The alloys were then exposed to room temperature (i.e. natural aging) for a total of 4 hours after the solution heat treatment. Subsequently the alloys were heat treated isothermally (i.e. artificial aging) at 185°C in an air circulation oven. The thermo-mechanical treatments for all the conditions are shown in Figure 1. Only the middle part of the samples (where the 1% pre-deformation was expected to be homogeneous) was used for further characterization for conditions (c) and (d).

Vickers hardness measurements were carried out on the cross-sectional surface of slices cut transversal to the extrusion direction. A Struers Durascan-70 machine was used for the hardness measurement. The hardness indenter was used with 5 kg load and a loading time for 15 seconds. Each data point corresponds to the average of ten hardness indentations, with the corresponding standard error.

TEM specimens were prepared by electro polishing with a Tenupol 5 machine (Struers, Denmark), on the transversal slices used for the hardness measurements. The electrolyte consisted of 1/3 HNO_3 in methanol and the solution was kept at temperatures between -20°C and -35°C.

Investigations of precipitate microstructure were performed by TEM in bright field mode using a Philips CM30 operating at 150 kV. A Gatan parallel electron energy loss spectroscopy (PEELS) was used to measure thickness of the specimens, i.e. in the center of the area used in each image. All the TEM and PEELS analyses were performed with the incident electron beam along the <001>Al directions where approximately 1/3 of the needles can be viewed in cross-section and 2/3 can be imaged perpendicular to the precipitate needle lengths. A combination of the bright-field TEM images with corresponding thicknesses enabled average precipitate needle-lengths, cross-sections, number densities and volume fractions to be quantified. A full description of the methodology has been given elsewhere [5, 38]. The total number of precipitate lengths and cross-sections measured were roughly 2000 and 700 respectively, for the statistical analysis in each thermo-mechanical condition. Widths of precipitate free zone (PFZ) adjacent to grain boundaries were measured from the TEM bright-field images.

3. Results

3.1 Hardness curves

Figure 2 shows hardness curves as a result of isothermal heat treatment at 185°C for different times up to 24 hours for the LC1, LC2 and LC3 alloys for the different thermo-mechanical treatments described above. The following are observations from Figure 2.

- The overall hardness of the LC3 alloys is consistently higher than that of the LC1 and LC2 alloys in all conditions. This suggests that a 0.1 wt% Cu addition significantly increases the hardness, which is in good agreement with previous results [11]. This strength increase is more

pronounced when peak hardness is reached as compared to the early stages of precipitation. The main reason for this difference must be the different hardness contributions: mainly solute hardening at early stages, while a gradual precipitation hardening increase towards the peak hardness.

- During the early stages of clustering/precipitation (before 2 hours of isothermal heat treatment), the hardness increases faster in the LC3 alloy in all conditions as compared to the LC1 and LC2 alloys, which indicates an accelerated precipitation kinetics due to 0.1 wt% Cu.
- Hardness curves for the LC1 and LC2 alloys are similar for all conditions. This suggests that a level of Cu additions of 0.01 wt% and below does not affect the precipitation hardening.
- The maximum hardness reached for each alloy is almost similar regardless of the quench rate and the 1% pre-deformation, although it was slightly lower in conditions (c) and (d). Faster hardness evolution was observed in the early stage for the conditions (c) and (d), which indicates accelerated precipitation kinetics in the 1% pre-deformed conditions.
- A tendency to double peak hardness evolution is observed in the LC1 and LC2 alloys in all conditions, being most pronounced in the condition (b). This effect is weaker in the LC3 alloy.
- The onset of the first hardness peak seems to be delayed for the LC1 and LC2 alloys in the conditions (c) and (d), and its value is higher than that of the second peak.
- In the condition (b), hardness starts to decrease after about 9 hours of aging for all alloys as compared to the other conditions, which indicates a faster over-aging.

3.2 Precipitate microstructure and precipitate free zone (PFZ)

The microstructure of the LC1 and LC3 alloys for 2 and 12 hours of isothermal heat treatment was investigated by bright-field TEM (the respective isothermal heat treatment times are indicated by vertical dashed lines in the hardness curves in Figure 2). Representative examples of bright-field TEM images are shown in Figure 3. Precipitates are present in form of needle-shaped with the main growth direction along <001>Al. The precipitates were identified to be mostly β” in the LC1 alloy and to be in coexistence with β” with a partially disordered structure in the same precipitate needle in the LC3 alloy at peak hardness condition [11]. The corresponding precipitate statistics (needle lengths, number densities, cross sections and volume fractions) are summarized in Figures 4 and 5. In all conditions, the LC3 alloy has finer precipitate microstructure characterized by higher number densities of shorter precipitates and consequently higher volume fractions as compared to the LC1 alloy. Apart from this observation, tendencies of the differences in the precipitate statistics depend on each thermo-mechanical condition – but are qualitatively the same, irrespective of the amount of Cu, see red dashed lines for the corresponding conditions in Figures 4 and 5. Increases in needle lengths and cross sections between 2 and 12 hours of isothermal heat treatment were most pronounced in the condition (b) as compared to the other conditions. As a consequence, increases in volume fractions were also most pronounced in the condition (b), since volume fraction is related to needle length, cross section and number density. Here, a very slight increase in number densities for the LC1 alloy and a decrease for the LC3 alloy can be observed between 2 and 12 hours of isothermal heat treatment. These observations indicate faster over-aging in the condition (b). This is in good agreement with the observations from the hardness curves shown in Figure 2. Needle lengths and cross-sections in the conditions (c) and (d) were longer and larger, respectively, than those in the condition (a) and (b) for both alloys. This shows that the 1% pre-deformation leads to faster growth of the precipitates.

Widths of PFZs adjacent to grain boundaries were measured from bright-field TEM images for each alloy and each condition. Examples of the PFZs on the TEM images are shown in Figure 6 and measurements of the widths of the PFZs are summarized in Figure 7. The PFZ widths in the LC3 alloys were narrower than those in the LC1 alloys for all conditions. This indicates that the Cu addition (~0.1wt%) leads to a reduction of the PFZs. In the conditions (b) and (d), wider PFZs were observed as compared to the conditions (a) and (c). This is a typical effect of the slow cooling on the PFZs [14]. However, the widths in the condition (d) were slightly narrower than those in the condition (b), which may be attributed to the 1% pre-deformation applied in the condition (d).

4. Discussion

It is demonstrated that influence of a Cu content of 0.01 wt% and below on hardness is negligible; the hardness curves for the LC1 and LC2 alloys were similar even including a distinct double peak hardness evolution in the condition (b). However a Cu content of ~0.1 wt% significantly affects the hardness in all the thermo-mechanical treatments. The addition of ~0.1 wt% Cu leads to higher hardness corresponding to higher number densities of shorter precipitates, which is in good agreement with our previous study [11]. Interestingly, these observations were made not only for the quenched condition (the condition (a)) but also for the slow cooling, the 1% pre-deformation and combination of these conditions (the conditions (b), (c) and (d)).

The exact cause of the double peak hardness evolution could not be determined with the experimental data acquired in this work. However, a similar double peak has previously been reported [5, 39, 40], although it was in a denser alloying element, a Si-rich alloy in a quenched condition, which was related to the formation of an earlier phase, called pre-β". Namely, the double peak corresponds to a transition of pre-β" to β" precipitates. The observed double peak hardness evolution in the present study could also be due to the same transition. It is noteworthy that it was observed in leaner, more Mg-rich alloys in slow cooling condition in the present study. The slow cooling, which generally leads to a lower quenched-in vacancy concentration, made this peak pronounced (the condition (b)). It may be speculated that formation of β" precipitates could be delayed because of lower vacancy concentrations creating a low nucleation rate for β" precipitates. As a consequence, a distinct double peak and corresponding increase in needle lengths and cross sections could be observed in the condition (b). The slow cooling rate also makes over-aging faster, which could be explained by lower vacancy concentrations (less atomic diffusion) to grow β" precipitates for long aging time because of a lack of available solute elements. These explanations can be supported by the fact that quench-in vacancies are required the formation of β", i.e. they form clusters transforming to β" [21]. Interestingly, a combination of slow cooling rate and 1% pre-deformation (the condition (d)) makes the double peak hardness evolution less pronounced. This may indicate that the formation of β" precipitates in the condition (d) is faster than that in the condition (b). It has been reported [33-36] that pre-deformation leads to acceleration of the formation of β" precipitates, which is due to reduced activation energy. It is plausible to suggest that the 1% pre-deformation leads to faster atomic diffusion and growth of β" precipitates, which can also be supported from the observation of the faster hardness evolutions in the conditions (c) and (d), see Figures 2. These observations indicate that the double peak is less pronounced when more energy is added to the system: either in the form of more quenched-in vacancies, pre-deformation or a combination of both which

promote atomic diffusion leading to formation of β". These explanations are illustrated in Figure 8.

Cu makes the effect of the double peak hardness less pronounced. This might be related to the observation that Cu is not entering the β" phase, but rather forms its own disordered structures [11, 12] which are less coherent with lower bulk energies. In addition, Cu makes higher number density of precipitates. These might make them less susceptible to the available vacancy amounts. It is suggested that Cu could make a compensation of low vacancy concentrations to make the double peak hardness less pronounced.

1% pre-deformation did not lead to a significant increase in hardness, as compared to e.g. 10%-15% pre-deformation [11, 27, 28]. It is suggested that the level of pre-deformation (~1%) does not give any notable work-hardening effect because of the relatively low dislocation densities, consistent also with the fact that the hardness in the as quenched stage is almost the same in all conditions. However, these dislocations *affect* atomic nucleation and precipitation, which is probably because they promote faster atomic diffusion in the 1% pre-deformed conditions. The 1% pre-deformation could potentially compensate the negative effects of slow cooling rate on the alloy properties. For example it *reduced* the effect of over-aging and of wider PFZs due to the slow cooling rate, as shown in the present study.

As mentioned, it is worth noting that Cu addition (~0.1 wt%) made PFZs narrower. A similar observation was reported in an alloy having ~0.5 wt% Cu [41], and also Ag in Al-Zn-Mg alloys [42]. This was because Ag has strong interaction with other alloying elements, which prevents solute depletion adjacent to grain boundaries, i.e. the critical vacancy concentrations for nucleation decreases [42]. It can be suggested that the ~0.1 wt% Cu addition also leads to decreasing the critical vacancy concentrations for nucleation in the region adjacent to grain boundaries since Cu can make high number densities of precipitates [11] due to own preferential atomic configuration [12]. These observations suggest that Cu additions could also compensate the effects of slow cooling rate on the alloy properties.

5. Conclusion

The influences of Cu additions (up to 0.1 wt%), quench rate and 1% pre-deformation on precipitation hardening in Al-Mg-Si alloys have been investigated. The highest Cu addition increases hardness of alloys with higher number densities of shorter precipitates, and reduces the width of PFZs. The effects of Cu were independent of the quench rate and the 1% pre-deformation. A double hardness peak observed during isothermal heat treatment is most probably due to the transition of pre-β" to β" precipitates, which was most pronounced in the slow cooling condition and less pronounced in the alloy with 0.1wt% Cu. 1% pre-deformation also made this effect less pronounced. These observations may be due to lower vacancy concentration in the slow cooling condition leading to a delayed formation of β" precipitates. Moreover the Cu addition and the 1% pre-deformation compensate for the delay due to faster atomic diffusion. Maximum hardness is affected by 0.1wt% Cu addition, but it is independent of thermo-mechanical treatments: slow cooing, the 1% pre-deformation and the combination of these. Although the slow cooling led to wider PFZs, this effect was less pronounced by the 1% pre-deformation and the 0.1wt% Cu addition. These observations can also be explained by faster atomic diffusion due to the 1% pre-deformation and the 0.1wt% Cu addition.

Acknowledgement

The authors would like to thank Dr. Olaf Engler, Hydro Bonn Germany, for composition measurement by inductively coupled plasma optical emission spectroscopy. This research is supported by Hydro Aluminum and the Research Council of Norway though the bilateral KMB project: 193619 “The Norwegian-Japanese Al-Mg-Si Alloy Precipitation Project”.

References

[1] E. Orowan, *The Institute of Metals, London*, Symposium on internal stresses in metals and alloys, 1948, 451-453.
[2] G.A. Edwards, K. Stiller, G.L. Dunlop, M.J. Couper, *Acta Mater.* 46 (1998) 3893-3904.
[3] S.J. Andersen, H.W. Zandbergen, J. Jansen, C. Træholt, U. Tundal, O. Reiso, *Acta Mater.* 46 (1998) 3283-3298.
[4] H.S. Hasting, A.G. Frøseth, S.J. Andersen, R. Vissers, J.C. Walmsley, C.D. Marioara, F. Danoix, W. Lefebvre, R. Holmestad, *J. Appl. Phys.* 166 (2009) 123527-1-123527-9.
[5] C.D. Marioara, S.J. Andersen, H.W. Zandbergen, R. Holmestad, *Metall. Mater. Trans. A* 36 (2005) 691-702.
[6] C.D. Marioara, H. Nordmark, S.J. Andersen, H.W. Zandbergen, R. Holmestad, *J. Mater. Sci.* 41 (2006) 471-478.
[7] R. Vissers, M.A. van Huis, J. Jansen, H.W. Zandbergen, C.D. Marioara, S.J. Andersen, *Acta Mater.* 55 (2007) 3815-3823.
[8] S. J. Andersen, C.D. Marioara, R. Vissers, A. Frøseth, H.W. Zandbergen, *Mater. Sci. Eng. A* 444 (2007) 157-169.
[9] S.J. Andersen, C.D. Marioara, A. Frøseth, R. Vissers, H.W. Zandbergen, *Mater. Sci. Eng. A* 390 (2005) 127-138.
[10] K. Matsuda, Y. Sakaguchi, Y. Miyata, Y. Uetani, T. Sato, A. Kamio, S. Ikeno, *J. Mater.Sci.* 35 (2000) 179-189.
[11] T. Saito, S. Muraishi, C.D. Marioara, S.J. Andersen, J. Røyset, R. Holmestad, *Metall. Mater. Trans. A* 44 (2013) 4124-4135.
[12] T. Saito, C.D. Marioara, S.J. Andersen, W. Lefebvre, R. Holmestad, *Philos. Mag.* 94 (2014) 520-531.
[13] D. Steele, D. Evans, P. Nolan, D.J. Lloyd, *Mater. Charact.* 58 (2007) 40-45.
[14] M. De Haas, T. Th. M. De Hosson, *J. Mater. Sci.* 37 (2002) 5065-5073.
[15] J.L. Cavazos, R. Colás, *Mater. Sci. Eng. A* 363 (2003) 171-178.
[16] J.W. Evancho, J.T. Staley, *Metall. Trans.* 5 (1974) 43-47.
[17] L.A. Girifalco, H. Herman, *Acta Metall.* 13 (1965) 583-590.
[18] S. Hirosawa, T. Sato, J. Yokota, A. Kamio, *Mater. Trans. JIM* 39 (1998) 139-164.
[19] H.S. Zurob, H. Seyedrezai, *Scripta Mater.* 61 (2009) 141-144.
[20] S. Pogatscher, H. Antrekwitch, H. Leitner, T. Ebner, P.J. Uggowitzer, *Acta Mater.* 59 (2011) 3352-3363.
[21] S. Pogatscher, H. Antrekwitch, H. Leitner, D. Pöschmann, Z.L. Zhang, P.J. Uggowitzer, *Acta Mater.* 60 (2012) 4496-4505.
[22] K. Strobel, M.A. Easton, L. Sweet, N.C. Parson, *Proceedinds of 13th International Conference on Aluminum Alloys (ICAA13)*, 3-7 June 2012, Pittsburgh, USA, ISBN 978-1-118-45804-4, pp. 1187-1192.

[23] M. Torsæter, H.S. Hasting, W. Lefebvre, C.D. Marioara, J.C. Walmsley, S.J. Andersen, R. Holmestad, *J. Appl. Phys.* 108 (2010) 073527-1-073527-9.
[24] J. Røyset, T. Stene, J.A. Saeter, O. Reiso, *Mater. Sci. Forum* 519-521 (2006) 239-244.
[25] H.J. Rack, *Mater. Sci. Eng.* 29 (1977) 179-188.
[26] H.-L. Lee, W.-H. Lu, S. L. Chan, *Scripta Metall. Mater.* 25 (1991) 2165-2170.
[27] K. Matsuda, H. Gamada, Y. Uetani, S. Rengakuji, F. Shinagawa, S. Ikeno, *J.J.I.L.M.* 48 (1998) 471-475.
[28] K. Matsuda, S. Shimizu, H. Gamada, Y. Uetani, F. Shinagawa, S. Ikeno, *J. Soc. Mater. Sci. Jpn.* 49 (1999) 10-15.
[29] K. Teichmann, C.D. Marioara, S.J. Andersen, K.O. Pedersen, S. Gulbrandsen-Dahl, M. Kolar, R. Holmestad, K. Marthinsen, *Philos. Mag.* 91 (2011) 3744-3754.
[30] K. Teichmann, C.D. Marioara, S.J. Andersen, K. Marthinsen, *Metall. Mater. Trans. A* 43 (2012) 4006-4014.
[31] R.S. Yassar, D.P. Field, H. Weiland, *Scripta Mater.* 53 (2005) 299-303.
[32] R.S. Yassar, D.P. Field, H. Weiland, *Metall. Mat. Trans. A* 36 (2005) 2059-2065.
[33] G.K. Quainoo, S. Yannacopoulos, *J. Mater. Sci.* 39 (2004) 6495-6502.
[34] Y. Birol, *Scripta Mater.* 52 (2005) 169-173.
[35] Y. Birol, M. Karlik, *Scripta Mater.* 55 (2006) 625-628.
[36] T. Matsuda, Y. Takaki, T. Sakurai, S. Hirosawa, *Mater. Trans.* 51 (2010) 325-332.
[37] A. Serizawa, T. Sato, M.K. Miller, *Mater. Sci. Eng. A* 561 (2013) 492-497.
[38] S.J. Andersen, *Metall. Mater. Trans. A* 26 (1995) 1931-1938.
[39] C.D. Marioara, S.J. Andersen, J. Jansen, H.W. Zandbergen, *Acta Mater.* 49 (2001) 321-328.
[40] C.D. Marioara, S.J. Andersen, J. Jansen, H.W. Zandbergen, *Acta Mater.* 51 (2003) 789-796.
[41] K. Matsuda, K. Kido, T. Kawabata, Y. Uetani, S. Ikeno, *J. J.I.L.M.* 53 (2003) 528-533.
[42] T. Ogura, S. Hirosawa, T. Sato, *Sci. Tech. Adv. Mater.* 5 (2004) 491-496.

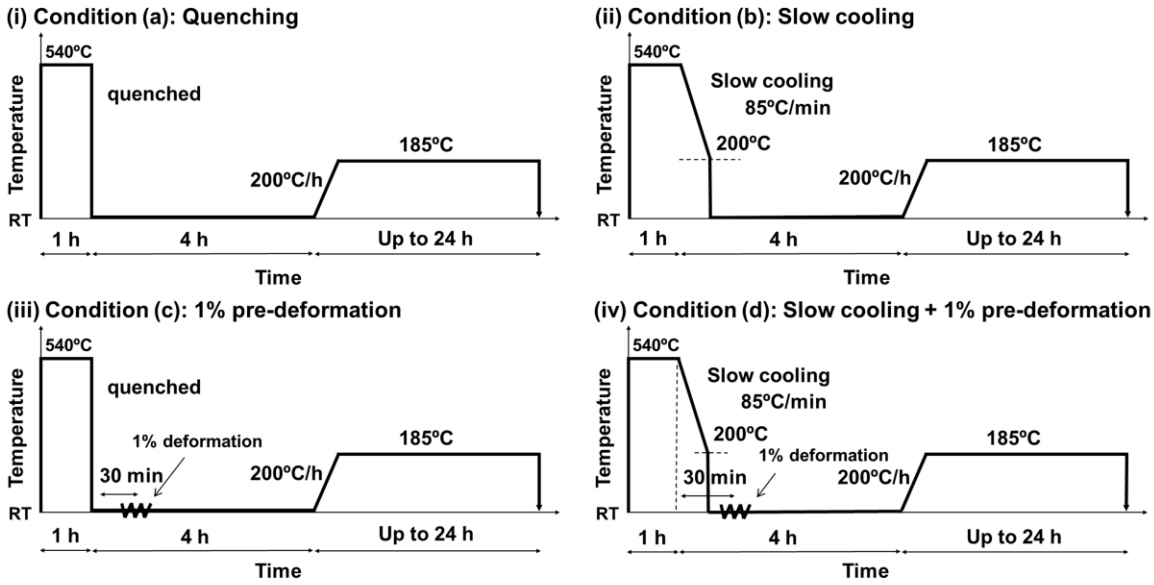

Figure 1 Thermo-mechanical histories for (i) Condition (a): quenching, (ii) condition (b): slow cooling, (iii) condition (c): 1% pre-deformation and (iv) condition (d): combination with the slow cooling and the 1% pre-deformation after solution heat treatment. The alphabetic designations correspond to Figures 2, 4, 5 and 8.

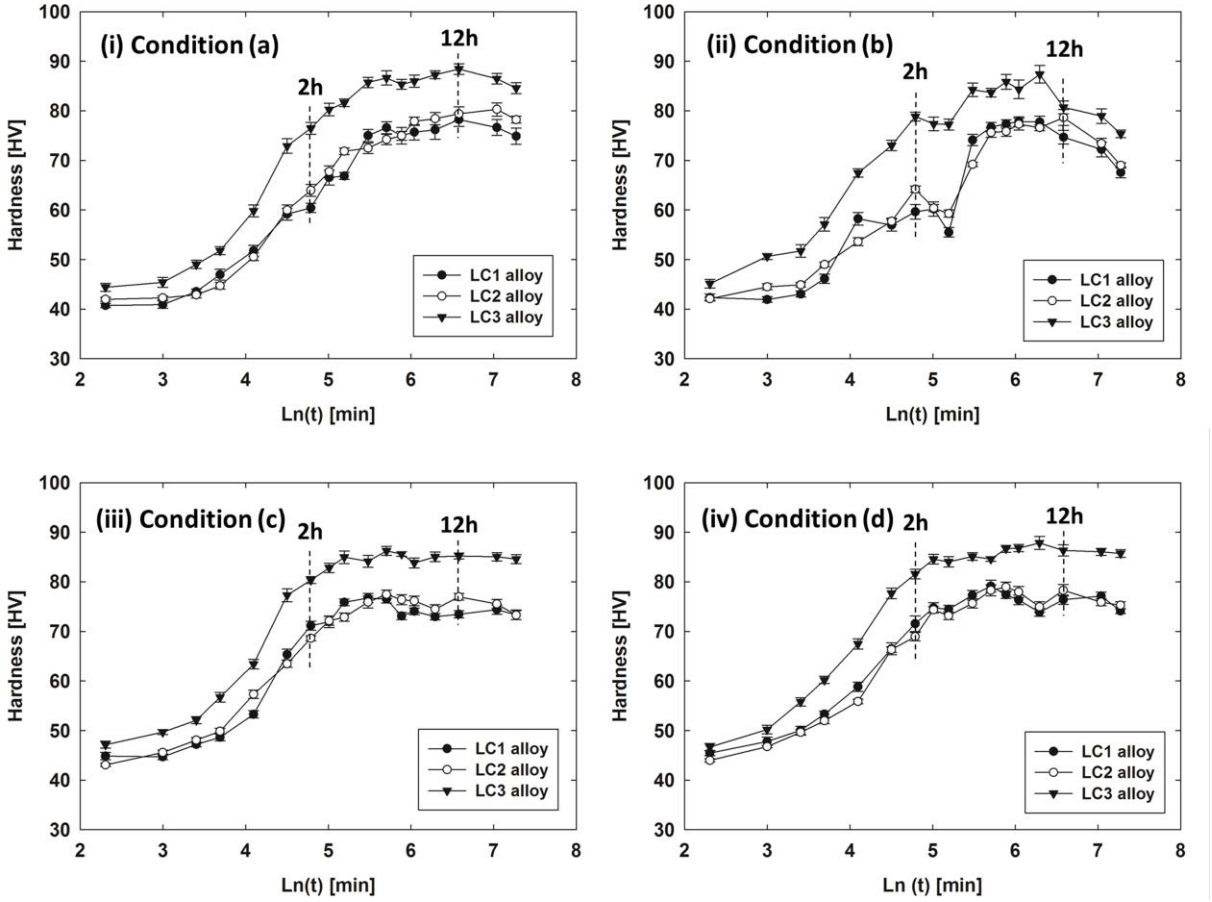

Figure 2 Hardness curves as a function of isothermal heat treatment times for the LC1, LC2 and LC3 alloys for (i) condition (a), (ii) condition (b), (iii) condition (c) and (iv) condition (d). The alphabetic designations for the thermo-mechanical treatments correspond to Figure 1. The alloy designations correspond to Table 1.

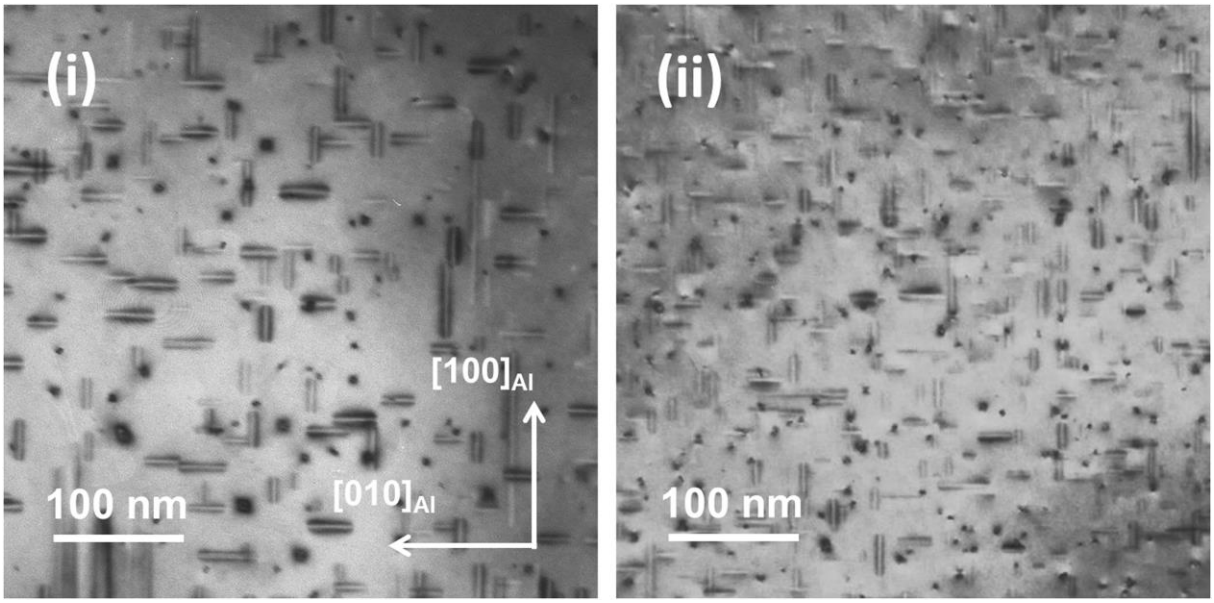

Figure 3 Examples of bright-field TEM images, which were used for taking precipitate statistics shown in Figures 4 and 5. The images shown were taken along <001>Al for (i) the LC1 and (ii) the LC3 alloys after isothermal heat treatment for 2 hours in the condition (a). The images are recorded in areas with similar thickness (50-70 nm) and with the same scale. Dark spots represent cross sections of the needle-shaped precipitates in the viewing direction.

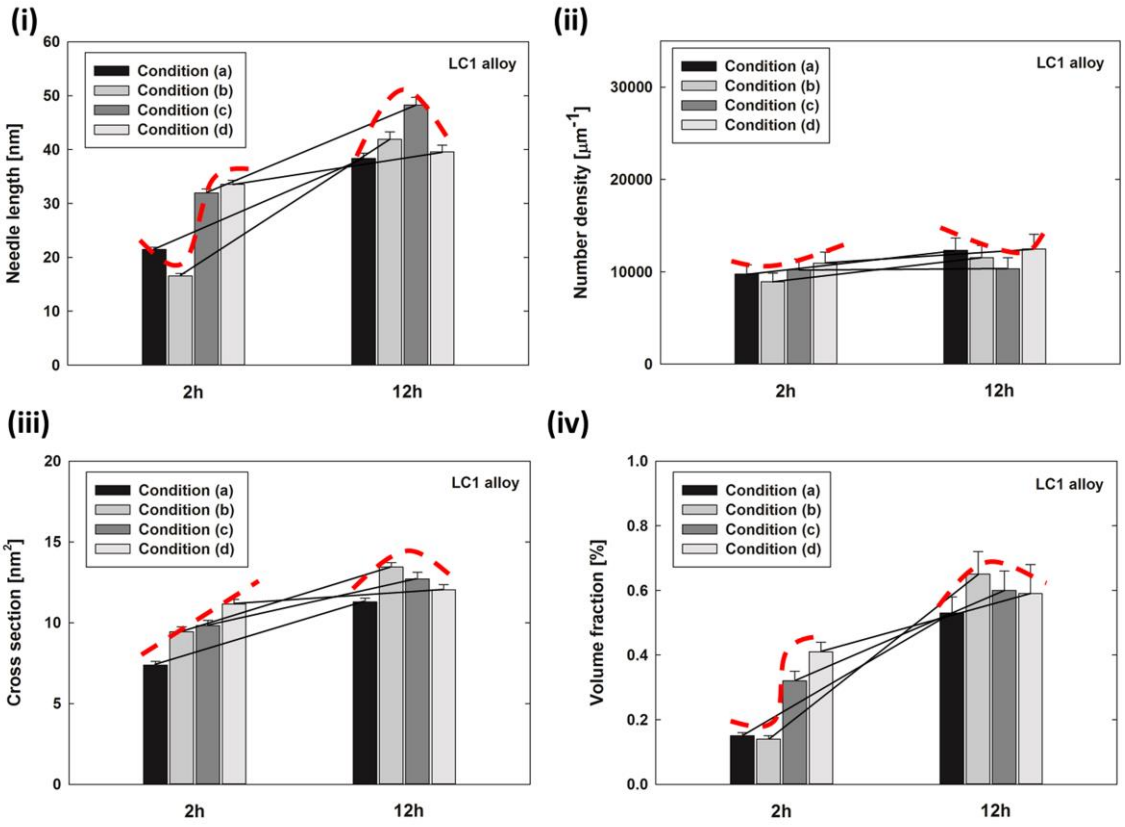

Figure 4 Precipitate statistics for the LC1 alloy after isothermal heat treatment for 2 and 12 hours in all conditions, calculated from a combination of bright-field TEM images and thickness measured by EELS. (i) Needle lengths, (ii) number densities, (iii) cross sections and (iv) volume fractions. The alphabetic designations for the thermo-mechanical treatments correspond to Figure 1. The alloy designations correspond to Table 1. Black solid lines connect each condition for 2 and 12 hours of isothermal heat treatment. Red dashed lines represent tendencies of differences in each condition.

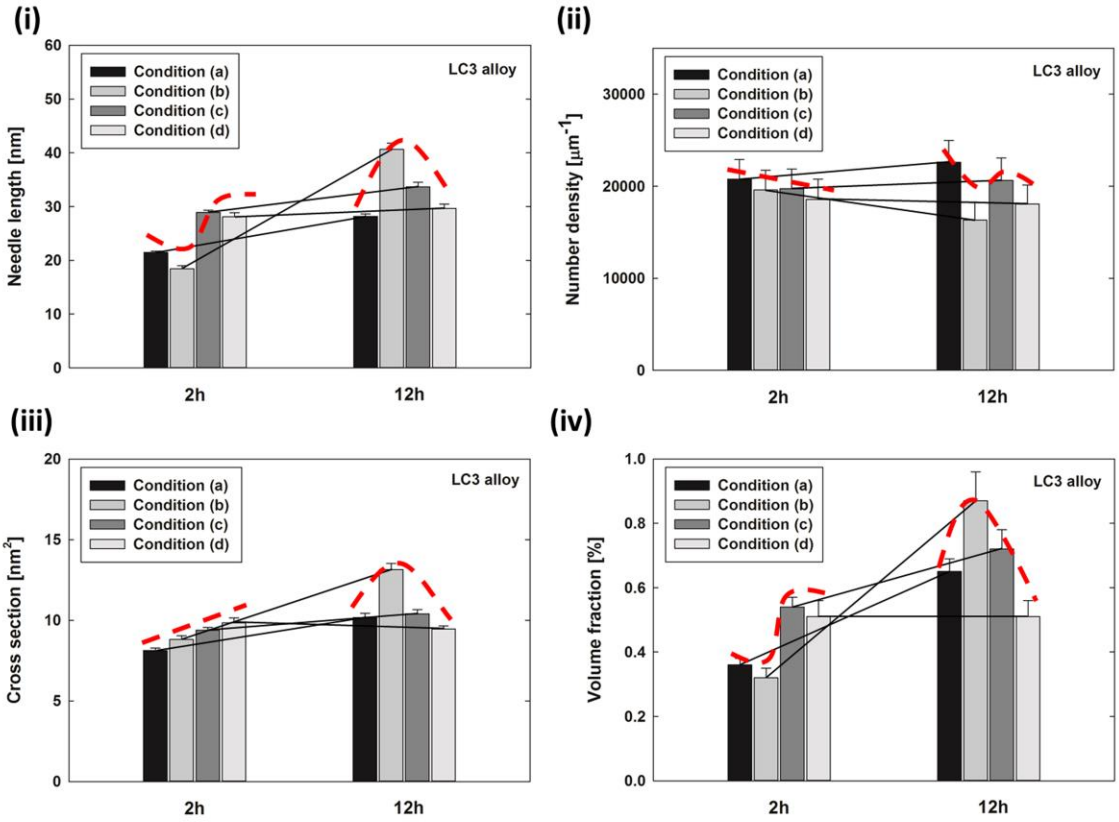

Figure 5 Precipitate statistics for the LC3 alloy after isothermal heat treatment for 2 and 12 hours in all conditions, calculated from a combination of bright-field TEM images and thickness measured by EELS. (i) Needle lengths, (ii) number densities, (iii) cross sections and (iv) volume fractions. The alphabetic designations for the thermo-mechanical treatments correspond to Figure 1. The alloy designations correspond to Table 1. Black solid lines connect each condition for 2 and 12 hours of isothermal heat treatment. Red dashed lines represent tendencies of differences in each condition.

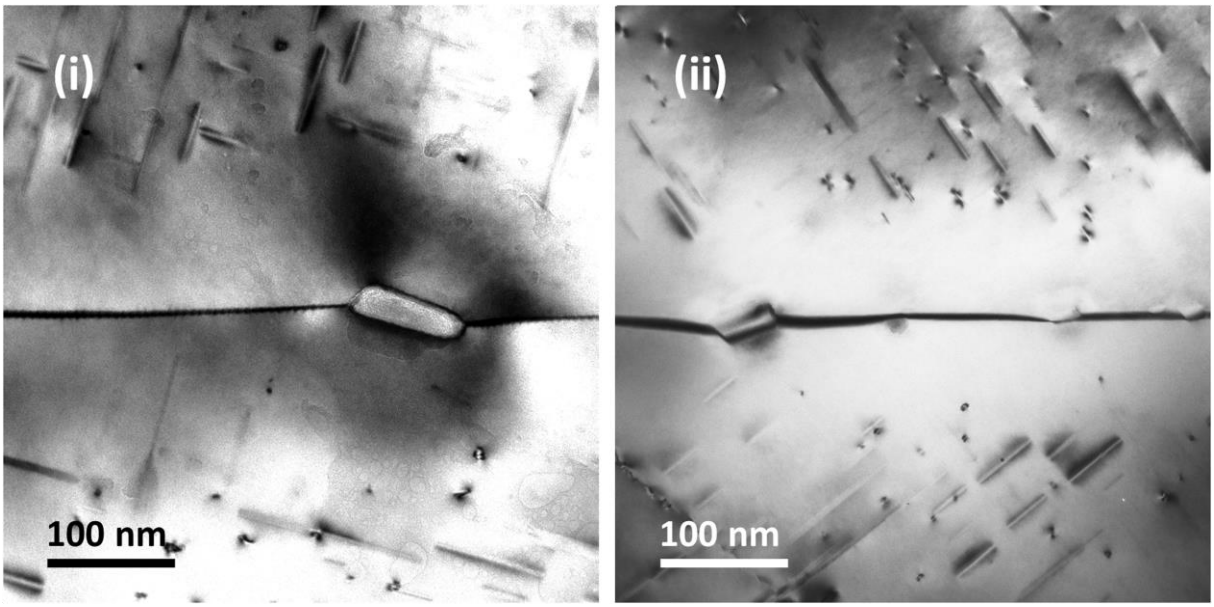

Figure 6 Examples of PFZs adjacent to a grain boundary taken by bright-field TEM images. The images shown were taken for (i) the LC1 alloy and (ii) the LC3 alloy after isothermal heat treatment for 12 hours in the condition (a). Precipitate needles and a grain boundary precipitate can be seen on grains and on the grain boundary, respectively. The images were recorded at the same scale.

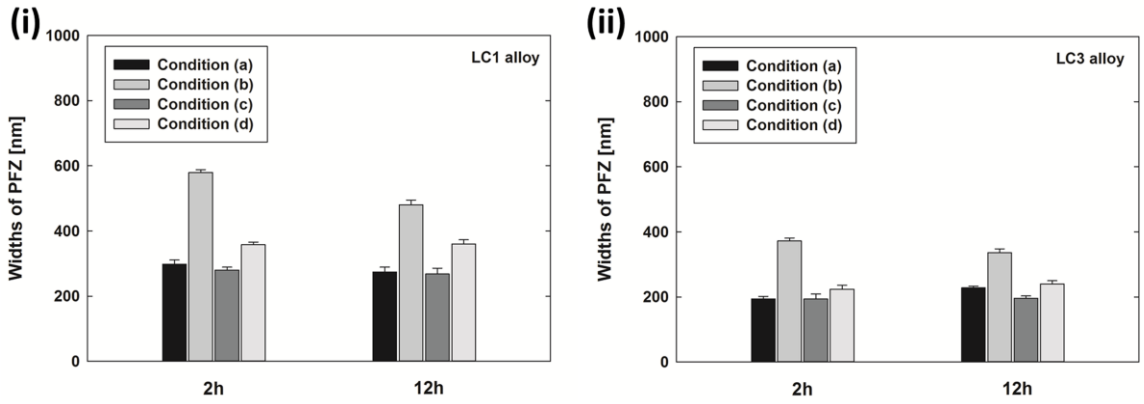

Figure 7 Widths of PFZ for (i) the LC1 and (ii) the LC3 alloys after isothermal heat treatment for 2 and 12 hours in all conditions. The alphabetic designations for the thermo-mechanical treatments correspond to Figure 1. The alloy designations correspond to Table 1.

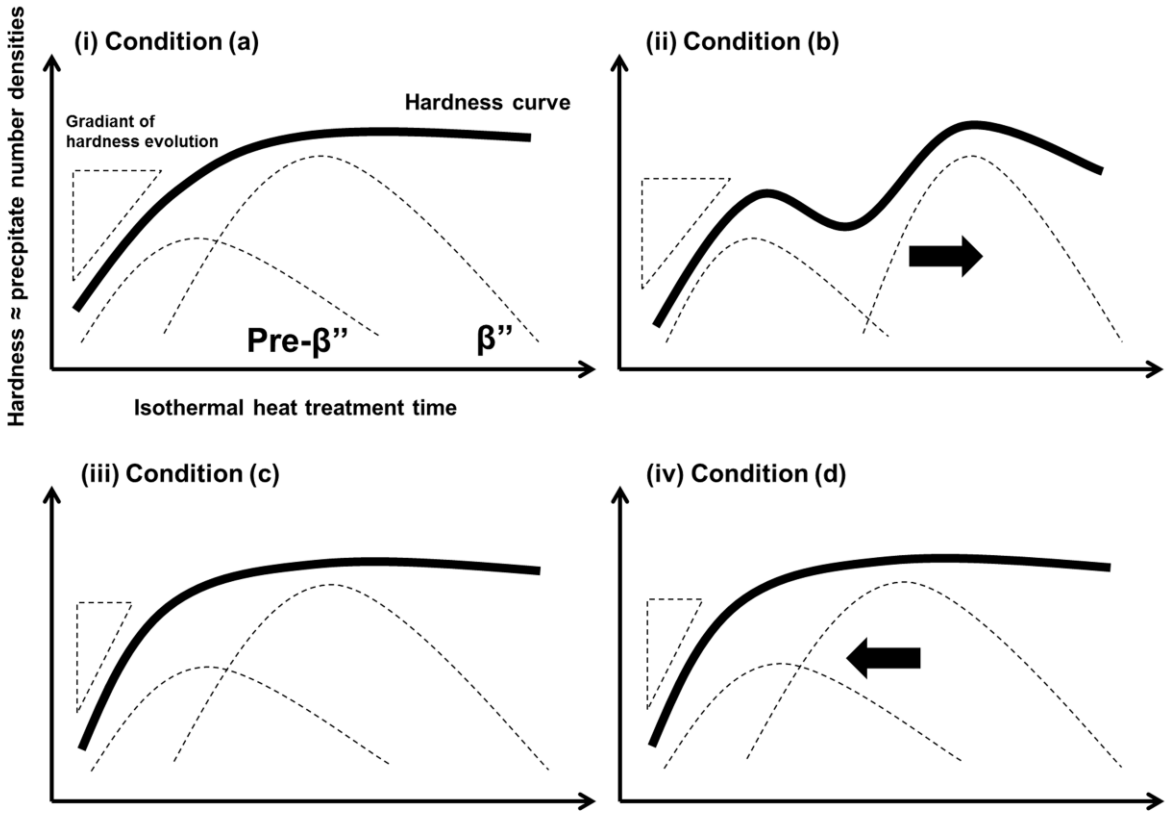

Figure 8 Schematic images of hardness curves corresponding to formation of pre-β” and β” precipitates for different thermo-mechanical treatments: (i) condition (a), (ii) condition (b), (iii) condition (c) and (iv) condition (d). The alphabetic designations correspond to Figure 1. Dashed triangles and lines represent gradient of hardness evolutions at early stages of precipitation and number of pre-β” and β” precipitates, respectively. An increase in hardness is related to number densities of the precipitates.